Iranian Journal of Geophysics, Vol 20 No 6, 2027, Page 49 – 73 (Research Article)
DOI: 10.30499/ijg.2025.534636.1715

Rock physics modeling of the effect of petrophysical parameters on seismic wave attenuation due to squirt flow in porous fractured media based on the T-matrix method

Mohammadfarid Ghasemi[1]*and Hadi Alimohammadi[2]

[1] *Assistant Professor, Shahid Beheshti University, Faculty of Earth Science, Tehran, Iran*
[2] *M.Sc., Shahid Beheshti University, Faculty of Earth Science, Tehran, Iran*

(Received: 15 July 2025, Accepted: 17 September 2025)

Summary

This study develops a comprehensive theoretical framework for quantifying frequency-dependent seismic attenuation in porous fractured carbonate rocks by integrating pore-scale microstructural characteristics with fluid saturation dynamics using the T-matrix approach. The model establishes an explicit connection between the hydraulic permeability tensor and ellipsoidal crack geometries, incorporating this relationship into a unified squirt flow formulation to predict both velocity dispersion and attenuation characteristics. Through systematic sensitivity analysis, the research demonstrates that permeability reaches maximum values in prolate-shaped cracks, while both attenuation patterns and velocity behavior are predominantly controlled by specific crack geometries and fluid composition properties. In single-phase fluid systems, increasing oil saturation produces elevated attenuation levels within typical logging frequency ranges of 1-20 kHz. In two-phase oil-gas systems, gas saturation below 20% induces substantial reduction in P-wave velocity along with increased attenuation effects, primarily resulting from significant compressibility contrasts between the fluid phases. The model validation utilized experimental data comprising five carbonate samples with complete petrophysical characterization. The inversion process for permeability estimation, employing a crack aspect ratio of 0.0001, demonstrated close alignment with experimentally measured values. Predicted quality factors (Q) showed strong correspondence with experimental attenuation measurements for homogeneous samples, though some deviations emerged in the heterogeneous sample where scattering effects presumably dominate over squirt-flow mechanisms. This research addresses a significant gap in existing models by establishing a direct microstructurally-based connection between permeability and dynamic squirt-flow response in fractured carbonate systems. The methodology advances beyond conventional approaches by incorporating the full permeability tensor derived from realistic pore geometries rather than relying on simplified scalar permeability values derived from empirical correlations. The results underscore the critical importance of incorporating pore shape frequency effects, and proper fluid substitution models into including attenuation for seismic data interpretation. The study acknowledges certain limitations in the current model, particularly its assumption of uniform fluid saturation and its inability to account for large-scale heterogeneities such as vugs and macro-fractures. These limitations are particularly relevant for complex carbonate reservoirs exhibiting multi-scale pore systems. Future work will focus on integrating patchy saturation effects for effective fluid modulus calculation, incorporating multi-scale pore inclusions representing different pore types, and combining the squirt-flow approach with scattering theory to better represent realistic porous-fractured environments. These enhancements will extend the model's applicability to more realistic geological formations. The framework presented here provides a foundation for developing more comprehensive rock physics models that can better address the challenges of characterizing heterogeneous carbonate formations through seismic attenuation analysis.

Keywords: Seismic wave attenuation, T-matrix model, fractured media, tight carbonates, reservoir characterization

*Corresponding author: mfghasemi110@gmail.com

1 Introduction

Seismic wave attenuation, quantified by the quality factor Q, arises from energy loss as waves propagate through rocks. Early models like the "Constant Q" theory (Kjartansson, 1979) reconciled frequency-dependent velocity dispersion with near-constant Q, linking phase velocity to frequency via a power-law relationship. This framework underscores the interplay between anelasticity and wave propagation, with nonlinear mechanisms (e.g., frictional sliding) dominating at high strains ($>10^{-6}$) and linear processes (e.g., fluid flow) prevailing at seismic strains ($<10^{-6}$) under confining pressures.

Attenuation mechanisms are broadly categorized into fluid-related, thermoelastic/phase-change, and solid-matrix processes. Fluid-related mechanisms dominate in saturated rocks, where Biot's theory (Biot, 1956) explains viscous dissipation from fluid-solid motion. However, microscale fluid flow—particularly squirt flow—between cracks and pores often surpasses Biot losses. Squirt flow, driven by pore pressure gradients in compliant cracks peaks at seismic frequencies and is amplified by partial saturation (Mavko and Nur, 1975), (Carcione et al., 2018a),(Alkhimenkov et al., 2020a), (Sun et al., 2020). Even trace fluids in cracks drastically lower Q (e.g., $Q \approx 100$) by enhancing pressure diffusion. White's model (White, 1975) is among first analytical models that links attenuation to fluid exchange between dry and saturated regions, predicting frequency-dependent Q inversely proportional to frequency. Strong evidence of squirt flow and the respective attenuation in real sandstone is reported by (Subramaniyan et al., 2015).

Thermoelastic dissipation (Savage, 1966), (Carcione et al., 2018b) and phase transitions (e.g., melt-vapor interactions) contribute to attenuation in dry or high-temperature rocks (Ricard et al., 2009), (Li, 2010) , while solid-matrix mechanisms like dislocation damping (Farla et al., 2012) and grain boundary relaxation (Jackson, 1971), (Buckingham, 2000) dominate in the mantle. External factors such as pressure, temperature, and microstructure modulate these processes, with crack density and connectivity generating a spectrum of relaxation times.

To probe these mechanisms, experimental methods span quasi-static to dynamic regimes. Quasi-Static Creep Tests (Quintal et al., 2011), (Coulman et al., 2013) measure time-dependent strain under steady stress, deriving the creep function J(t). Fourier transforms link J(t) to dynamic compliance J(ω), enabling extrapolation to seismic frequencies (Jackson and Paterson, 1993). The Andrade model ($J_a(t) = J_u + \beta t^m + t/\eta$) distinguishes recoverable (anelastic) and viscous strain, though nonlinearity at high strains complicates analysis (Goetze, 1977); among Dynamic Methods Ultrasonic Wave Propagation (100–900 kHz) infers attenuation from amplitude decay, assuming grain-boundary relaxation scaling (Sato, 1984). Resonance Methods analyze free oscillations (1–20 kHz) or pendulum setups (1–100 Hz) to measure Q^{-1}, though temperature-induced microstructural changes limit reliability (Gueguen et al., 1981). Forced Oscillation Experiments apply sinusoidal stress at subresonant frequencies (1–100 s periods), measuring phase lag δ to calculate $Q^{-1} =$

tan δ (Jackson et al., 1992). Torsional setups, compatible with high-pressure/temperature (HPHT) conditions, are favored for their sensitivity to modulus dispersion (Jackson and Paterson, 1993).

Among the abovementioned mechanisms squirt flow's role in attenuation has been refined through analytical, numerical, and experimental advancements. Among analytical models, Solazzi et al., (2021) derived a frequency-dependent fluid bulk modulus for partially saturated cracks, capturing viscous dissipation in gas-water systems. Validated against 3D simulations, this model bridges gaps in earlier saturation-limited theories. (Alkhimenkov et al., 2020b; Alkhimenkov and Quintal, 2021, 2024) proposed a simplified squirt flow model for isotropic rocks, demonstrating superior accuracy over predecessors by directly incorporating measurable pore geometry parameters. Additionally, Yang et al., (2007) linked pore size, crack length, and saturation paths to attenuation magnitude and characteristic frequency via dynamic stress-strain simulations, emphasizing fluid distribution's role in pressure diffusion. Experimental procedure can be integrated with Theoretical methods to investigate both the attenuation estimation and validation of the procedure used. (Ba et al., 2023; Ba et al., 2024) combined squirt flow with acoustoelasticity, showing how crack closure and fluid substitution reduce velocity-pressure dependence in carbonates. This reconciles microscale fluid dynamics with macroscale dispersion trends. The Biot-spherical squirt – BISSQ (Chen et al., 2022) unified Biot and spherical squirt flow, simulating P-wave attenuation under variable fluid viscosity and squirt length. Applied to Fox Hills Sandstone, it validated squirt flow's dominance in realistic settings.

Squirt flow has also been used in Hydrocarbon Exploration. Lan et al., (2023) introduced a viscoelastic squirt-flow fluid factor, enhancing fluid discrimination by mitigating "false bright spots" in seismic data. Field validations demonstrated higher vertical resolution, underscoring squirt flow's practical value in reservoir characterization. Squirt flow emerges as a linchpin in seismic attenuation, governed by pore geometry, fluid properties, and stress conditions. The integration of squirt flow with broader mechanisms—via models like BISSQ (Chen et al., 2022) and acoustoelasticity (Ba et al., 2024)—advances predictive capabilities across seismic to ultrasonic frequencies. However, a comprehensive model that explicitly links the full hydraulic permeability tensor, derived from realistic microstructural parameters, to frequency-dependent attenuation and dispersion in fractured, tight carbonates remains underdeveloped. This study aims to bridge this gap by developing a rigorous rock physics model based on the T-matrix method. Our approach critically extends previous work by: 1) Explicitly calculating the permeability tensor for a medium containing chaotically oriented ellipsoidal cracks and pores of varying aspect ratios. 2) Integrating this dynamic permeability into a unified squirt flow formulation to model frequency-dependent velocity dispersion and attenuation (Q^{-1}). 3) Performing a systematic sensitivity analysis to quantify the impact of pore geometry, fluid viscosity, and saturation (both single and two-phase) on seismic properties across a broad frequency

band.

By moving beyond historical simplifications, our model provides an analytical tool to potentially decode seismic attenuation data and directly invert for key reservoir quality parameters—such as porosity, permeability, and fluid composition—in fractured carbonate systems. The T-matrix approach employed in this study offers several fundamental advantages over alternative models like the Biot-spherical squirt (BISSQ) and acoustoelastic frameworks. Its primary strength lies in its microstructural foundation, which derives effective properties directly from the mechanics of inclusions, providing a clearer physical interpretation of the fluid-rock interaction than macroscopic stress-strain relationships. Crucially, the model ensures mass conservation and coupling consistency by unifying global (Biot) and local (squirt) flow processes within a single, self-consistent framework, thereby correcting a key theoretical shortcoming in models that treat these mechanisms separately (Diallo and Appel, 2000), (Jakobsen, 2007; Jakobsen and Chapman, 2009; Jakobsen et al., 2003). This formulation also addresses critical stability and well-posedness issues identified in certain BISSQ models, which can produce unphysical, exponentially growing solutions (Liu and Yong, 2016). Furthermore, the formalism naturally extends to anisotropic media, allowing for the explicit incorporation of fracture orientation and connectivity through a permeability tensor, a significant advancement for modeling real fractured reservoirs. Consequently, the T-matrix approach provides a, physically sound, and mathematically stable theoretical basis for predicting frequency-dependent attenuation in complex porous fractured rocksThe following manuscript is structured as follows: First, we introduce the necessary theoretical framework for computing squirt flow using the T-matrix formulation developed by Jakobsen and Chapman, (2009). In this formulation, hydraulic permeability is expressed as a second-rank tensor, which is directly related to the microstructural parameters of the constructed rock physics model. To estimate hydraulic permeability, we adopt the T-matrix-based approach proposed by (Barthélémy, 2009) and later expanded by (Jakobsen, 2007), leveraging the microstructural parameters derived from our rock physics model. Following this theoretical foundation, we construct a simplified rock physics model. Subsequently, we perform a sensitivity analysis to examine how variations in pore-space morphology and fluid saturation influence permeability, seismic wave velocity, and attenuation. To validate the theoretical results and ensure the proposed framework yields reliable predictions, we utilized experimental data from Adam (2009). The validation process involved the following steps: First, we solved an inverse problem using the permeability data from Adam (2009) to derive the crack aspect ratios. Subsequently, these inferred aspect ratios, along with other parameters reported in the same study, were used to estimate the inverse quality factor (Q^{-1}). Finally, the theoretically derived attenuation was compared to the experimental data by plotting both on a log-log scale. This plotting method was chosen to magnify any discrepancies and to facilitate a clearer resolution of the differences between the two datasets across the investigated frequencies for

the five carbonate samples.

2 Methodology

In the following section when we mention words in bold and plain text, we're talking about fourth-rank tensors. Words in italic and bold are used for second-rank tensors (3 by 3 matrix). And when we use just plain italic words, we're referring to scalars.

3 Modified Jakobsen's model for stiffness tensor calculation

Jakobsen and Hudson, (2003) compiled some of the existing effective medium models and formalized them to model the elastic properties of anisotropic shales by placing them on a T-matrix. Jakobsen and Hudson, (2003) represent the following equation for the effective elastic stiffness as,

$$\mathbf{C}_T^* = \mathbf{C}^{(0)} + \langle \mathbf{C}_1 \rangle : (\mathbf{I} - \langle \mathbf{C}_1 \rangle^{-1} : \mathbf{C}_2)^{-1}, \quad (1)$$

where

$$\langle \mathbf{C}_1 \rangle = \sum_{r=1}^{N} v^{(r)} \mathbf{t}^{(r)}, \quad (2)$$

$$\mathbf{C}_2 = -\sum_{r=1}^{N} \sum_{n=1}^{N} v^{(r)} \mathbf{t}^{(r)} \mathbf{G}_d^{(rn)} \mathbf{t}^{(n)} v^{(n)}, \quad (3)$$

and, $\mathbf{I}$ is the fourth-rank Identity tensor. The T-matrix ($\mathbf{t}^{(r)}$) for a single inclusion of elastic stiffness $\mathbf{C}^{(r)}$ is given by:

$$\mathbf{t}^{(r)} = \delta \mathbf{C}^{(r)} (\mathbf{I} - \mathbf{G}^{(r)} \delta \mathbf{C}^{(r)})^{-1}, \quad (4)$$

Where

$$\delta \mathbf{C}^{(r)} = \mathbf{C}^{(r)} - \mathbf{C}^{(0)}, \quad (5)$$

The fourth-rank tensor $\mathbf{G}^{(r)}$ is the second derivative of green's function and can be described as follow:

$$G_{pqrs}^{(r)} = -\frac{1}{4}\left[E_{pqrs}^{(r)} + E_{pqsr}^{(r)} + E_{qprs}^{(r)} + E_{qpsr}^{(r)}\right], \quad (6)$$

$$E_{pqrs}^{(r)} = \int_0^{\pi} d\theta sin\theta \int_0^{2\pi} d\phi D_{qs}^{-1}(k) k_p k_r A^{(r)}(\theta, \phi), \quad (7)$$

$$D_{qs} = C_{qmsn}^{(0)} k_m k_n, \quad (8)$$

Here, $C^{(0)}$is the stiffness tensor of the homogenous embedding medium which can be isotropic or anisotropic. To incorporate the impact of fluid flow in the inclusion and interaction of them with the embedding medium, and to accurately calculate the stiffness tensor of the medium, Jakobsen et al., (2003) and Jakobsen and Chapman, (2009) developed a lengthy derivation that resulted in the final equation, known as the t-matrix, for a communicating cavity:

$$\mathbf{t}^{(n)} = \mathbf{t}_d^{(n)} + \frac{\Theta \mathbf{Z}^{(n)} + i\omega\tau\kappa_f \mathbf{X}^{(n)}}{1 + i\omega\gamma^{(n)}\tau}, \quad (9)$$

where,

$$\mathbf{X}^{(n)} = \mathbf{t}_d^{(n)} : \mathbf{S}^{(0)} : (\mathbf{I}_2 \otimes \mathbf{I}_2) : \mathbf{t}_d^{(n)} : \mathbf{S}^{(0)}, \quad (10)$$

And

$$\mathbf{Z}^{(n)} = \mathbf{t}_d^{(n)} : \mathbf{S}^{(0)} : (\mathbf{I}_2 \otimes \mathbf{I}_2) : \left(\sum_{r=1}^{N_c} \frac{v^{(r)} \mathbf{t}_d^{(n)}}{1 + i\omega\gamma^{(r)}\tau} \right) : \mathbf{S}^{(0)}, \quad (11)$$

$$\Theta = (1 - \Delta)\left(\kappa_f \left[\sum_{r=1}^{N} \frac{\phi^{(r)} \gamma^{(r)}}{1 + i\omega\gamma^{(r)}\tau} (1 - \Delta) - \frac{i\kappa_f \Gamma_{ij} k_i k_j}{\eta_f \omega} \right]^{-1} \right) \quad (12)$$

where i, ω, τ, η_f, κ_f, $\gamma^{(n)}$are imaginary number, angular frequency (Hz), relaxation time (second), fluid viscosity, fluid bulk modulus, Pa, normalized compliance tensor (see equation 14). k_i is the component of the wave number vector, Γ_{ij} is i,j 'th companent of the 2nd-rank permeability tensor $\mathbf{X}^{(n)}$, $\mathbf{Z}^{(n)}$ and Θ are just extracted parameters to

simplify presenting equation 9, and do not present any specific physical concept. Based on the Jakobsen and Chapman, (2009), Δ is the term of the coupling between the processes of global flow and squirt flow as follow,

$$\Delta = \frac{\kappa_f \tau}{\phi \eta_f} \Gamma_{ij} k_i k_j , \quad (13)$$

and

$$\gamma^{(n)} = 1 + \kappa_f (K_d^{(n)} - S^{(0)})_{uuvv} . \quad (14)$$

where Einstein summation is employed on repeating indices. In the context of linear superposition as proposed by Mukerji and Mavko, (1994) and subsequent manipulation, Jakobsen et al., (2003) presented the K-matrix for a stress in the dry cavity of type n.

$$\mathbf{K}_d^{(n)} = (\mathbf{I}_4 + \mathbf{G}^{(n)} : \mathbf{C}^{(0)})^{-1} : \mathbf{S}^{(0)} , \quad (15)$$

and, by utilizing equation 12 and certain derivations pertaining to a communicating cavity that is fully saturated and able to exchange fluid mass with other cavities under local and global pressure gradients, the following equation for the T-matrix in the dry cavities can be derived:

$$\mathbf{t}_d^{(n)} = -\mathbf{C}^{(0)} : \left(\mathbf{I}_4 + \mathbf{G}^{(n)} : \mathbf{C}^{(0)}\right)^{-1} . \quad (16)$$

According to Hudson et al., (1996), the relaxation time – τ, is directly proportional to pore size and fluid viscosity, while inversely proportional to permeability. Chapman et al., (2002), in conjunction with the derivation of a microstructural poroelastic model, formulated the first equation for the relaxation time as follows:

$$\tau = \frac{4\eta_f r^3 (1-\upsilon)}{9\, \Gamma \varsigma \mu}, \quad (17)$$

where, r is the crack radius (m), υ is the Poisson ratio, ς is the grain size (m), μ is shear modulus (Pa), η_f is the fluid viscosity (Pa.s), and the Γ is the average permeability in three direction $\Gamma = \frac{\Gamma_{11}+\Gamma_{22}+\Gamma_{33}}{3}$ permeability (m^2). The proportionality constants in Eq. 17 arise from the analytical solution for viscous fluid flow within a penny-shaped crack. The factor of 4/9 and the term (1-ν) are derived from integrating the fluid flux required to equilibrate a pressure differential across the crack's surface, relating it to the macroscopic deformation via Hooke's law. This formulation, established by Chapman et al. (2002), is fundamental to models describing squirt flow in compliant crack geometries.

In order to incorporate the impact of pore fluid on the effective stiffness tensor, it is imperative to homogenize the fluid component and take into consideration the collective influence of all fluid components on the ultimate tensor.Wood, (1957) introduced an adapted formula for calculating the fluid's bulk modulus within an isostress model, recognized as the Ruess formula.

$$\frac{1}{K_R} = \sum_{i=1}^{N} \frac{f_i}{K_i} . \quad (18)$$

Here K_R, f_i and K_i are bulk modulus of homogenized fluid (mixture of fluids saturating the pore space), i^{th} fluid saturation and i^{th} fluid bulk modulus respectively. When pore fluids are present as distinct patches rather than being uniformly distributed, the effective bulk modulus may exceed predictions based on Wood's law (Carcione and Avseth, 2015).

4 Permeability estimation based on T-matrix method

To analyze conductivity, we adhere to the methodologies delineated by Sævik et al., (2012); (Sævik et al., 2013; Sævik et al., 2014), which draw heavily from the foundational work of Torquato,

(2002) and Barthélémy, (2009). These studies evaluate various effective medium models designed to predict the effective conductivity (hydraulic, electrical, and electromagnetic) of porous media. The models under consideration include Maxwell's approximation (Torquato, 2002), symmetric and asymmetric self-consistent approximations (Fokker, 2001), differential effective medium approximation (Torquato, 2002), and the T-matrix method (Jakobsen, 2006). Notably, the T-matrix and the symmetric and asymmetric self-consistent methods demonstrated greater consistency with the laminated bounds used to validate these methods across different fracture densities. The T-matrix formulation to estimate the effective conductivity of a porous medium is as follow (Jakobsen, 2006; Sævik et al., 2014):

$$\boldsymbol{R}^{*} = \boldsymbol{R}^{(0)} + \boldsymbol{R}_1 \cdot \left(\boldsymbol{I}^{(2)} + \boldsymbol{G}^{(r)} \cdot \boldsymbol{R}_1\right)^{-1}, \tag{19}$$

$$\boldsymbol{R}_1 = \langle \boldsymbol{r}^{(r)} \rangle, \tag{20}$$

where, $\boldsymbol{R}^{*}$, $\boldsymbol{R}^{(0)}$ are effective conductivity and conductivity of the embedding matrix. Again, we emphasize that, conductivity, encompasses electrical, electromagnetic, and hydraulic conductivity. $\boldsymbol{I}^{(2)}$ is the second rank unity tensor (a 3 by 3 matrix, with diagonal elements equal to one and other elements equal to zero). $\langle . \rangle$ means the average over spatial orientation and volumetric concentration. $\boldsymbol{t}^{(r)}$ is the t-matrix of inclusions of type *(r)* and can be defined as:

$$\boldsymbol{r}^{(r)} = \left(\boldsymbol{R}^{(r)} - \boldsymbol{R}^{(0)}\right) \cdot \left[\boldsymbol{I}^{(2)} - \boldsymbol{G}^{(r)} \cdot \left(\boldsymbol{R}^{(r)} - \boldsymbol{R}^{(0)}\right)\right]^{-1}, \tag{21}$$

where, $\boldsymbol{R}^{(r)}$ and $\boldsymbol{G}^{(r)}$ are the inclusion conductivity and field concertation tensors, respectively. $\boldsymbol{G}^{(r)}$, referred to as $\boldsymbol{P}^{(0)}$ in Barthélémy's original paper can be estimated using a complex numerical method described in his work. The method presented by Bayuk and Chesnokov (1998) is similar to the field concentration tensor for the effective elastic tensor discussed in equations (7) to (12), and can also be used to estimate $\boldsymbol{G}^{(r)}$ (Bayuk and Chesnokov, 1998):

$$G_{ij} = -\frac{1}{4\pi}\int_0^{2\pi}\int_0^{\pi}(n_{ij}\Lambda^{-1})\sin\theta d\theta d\varphi, \tag{22}$$

$$\Lambda = R_{ij}^{(0)} n_{ij}, \tag{23}$$

where $\Lambda = R_{ij}^{c} n_{ij}$. n_1, n_2, n_3 are defined the same as equation. Einstein summation convention is used here that the repeating indices denote summing over 1,2,3. $R_{ij}^{(0)}$ is the transport tensor which is the effective electrical and hydraulic conductivity tensors of the comparison body. In case of hydraulic permeability the $\boldsymbol{R}$ notation should be replaced by the notation used in this manuscript indicating permeability i.e. $\boldsymbol{\Gamma}$.

Attenuation formulation:

The standard definition of attenuation as described by Jakobsen 2009 (Jakobsen and Chapman, 2009)can be depicted as follow:

$$\frac{1}{Q} = \frac{2\alpha V}{\omega} = \frac{\alpha V}{\pi f}, \tag{24}$$

in this equation, V is the phase velocity, α is the attenuation coefficient, ω is the angular frequency, and f represents the linear frequency ($\omega = 2\pi f$) .

In the current study our primary focus is on investigating the capabilities of the T-matrix model. Specifically, our objective is to thoroughly examine certain aspects of this theory. Our inquiry centers on applying the model to a fully saturated tight carbonate

medium, where both grain and pore sizes are significantly smaller than the wavelength. In elucidating fluid behavior in this context, we have employed Wood's law for fluid homogenization. The implications of the patchy saturation model within the effective medium theory would be investigated in separate research.

5 Result and discussions

As elucidated in the methodology section, for precise monitoring of medium properties through seismic waves, it is imperative that the wavelength significantly surpasses the scale of heterogeneity. Our model, grounded in the T-Matrix approach developed by Jakobsen and Hudson, (2003), necessitates the establishment of the following rule:

$\lambda \gg H > r$ as illustrated in Figure 1.

Considering the intricate relationships between the saturation of single-phase and two-phase fluids, the relaxation time of the fluid, the morphology of pores, as well as the speed and attenuation in porous materials, we examine these factors and their collective impact on the attenuation and velocity of compressional waves. Ultimately, through the resolution of inverse equations, we can accurately ascertain the real values of independent factors introduced at various depths beneath the surface, leveraging standard acoustic logs, as illustrated in Figure 2 To do so, we construct a simple rock physic model to perform sensitivity. First for the embedding matrix we consider calcite with bulk and shear moduli of 65 and 28 GPa, respectively, and a density of 2.71 g/cm³ as indicated in chapter 4 of Mavko et al., (2020). Then we place chaotically oriented ellipsoidal inclusions further also referred to as cracks and ellipsoidal cracks, with semi – axis a_1, a_2, and a_3 which are aligned with standard cartesian coordinate system axis x_1, x_2 and x_3. Therefore, two aspect ratios for ellipsoidal inclusions can be defined as $\alpha_3 = a_3/a_1$ and $\alpha_2 = a_2/a_1$. When α_3 or α_2 are greater than 1 the ellipsoidal inclusion is referred to as prolate inclusion and when their value is less than unity the inclusion is referred to as penny shape inclusion.

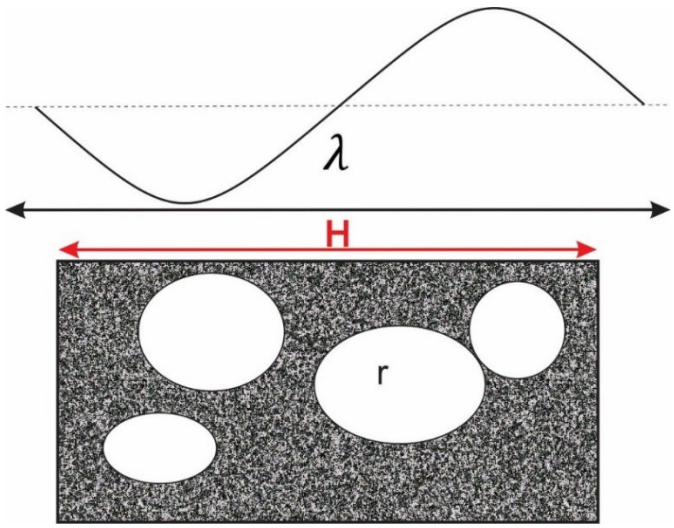

Figure 1. the schematic scheme in the mesoscopic model to define the comparison scale of the pores, frame of matrix, and wavelength.

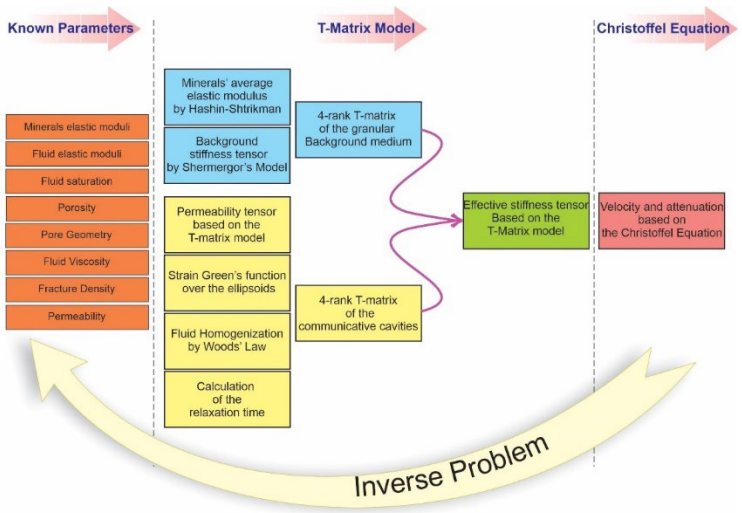

Figure 2. Schematic Representation of Our model in the T-matrix model and the inverse problem concept. We start by using the initial parameters of the porous medium as our known inputs. This allows us to measure key factors like the effective stiffness tensor, artificial velocities, and attenuation. In the final stage, we employ inverse problem methods.

Permeability:

Our results, illustrated in. Figure 3, are based on variations in the ellipsoidal inclusion semi-axis lengths. To align with other findings we further organized the results into three sections depicting permeability and attenuation responses to small, medium, and large sizes of the third axis. By small (or minimum) we mean $a_3 << a_1, a_2$, by medium we mean a_3 is a value between the selected sensitivity range for a_1 and a_2, and finally by large (or maximum) we mean $a_3 >> a_1, a_2$.

According to Figure 3 our model notably suggests that ellipsoidal cracks with a prolate shape yield the highest permeability values.

Saturation in single phase fluid:

Figure 4 to Figure 6 illustrate the impact of single-phase fluid presence on acoustic impedance, attenuation, and P-wave velocity.

Specifically, Figure 4 and Figure 5 showcase variations in acoustic impedance and compressional wave velocity as we vary single-phase saturation with two components of oil and water, spanning seismic to core frequency ranges, respectively. The oil percentage ranges from 0 to 60 percent, mirroring conditions akin to a real tight carbonate medium.

As depicted in Figure 5, an increase in fluid viscosity induces noticeable positive dispersion across all frequency ranges. This positive dispersion is particularly pronounced in scenarios of active global fluid flow at low frequencies, compared to medium and high frequencies where fluid flow is influenced by squirt flow.

Figure 6 elucidates how attenuation manifests due to fluctuations in single-phase fluid content across various frequencies, with the highest attenuation observed within the logging frequency range. A consistent correlation is observed between the increase in fluid viscosity or the percentage of oil in the single-phase fluid and the rise in attenuation. As illustrated in Figure 5 and Figure 6, P-wave velocity clearly decreases with fluid content, but

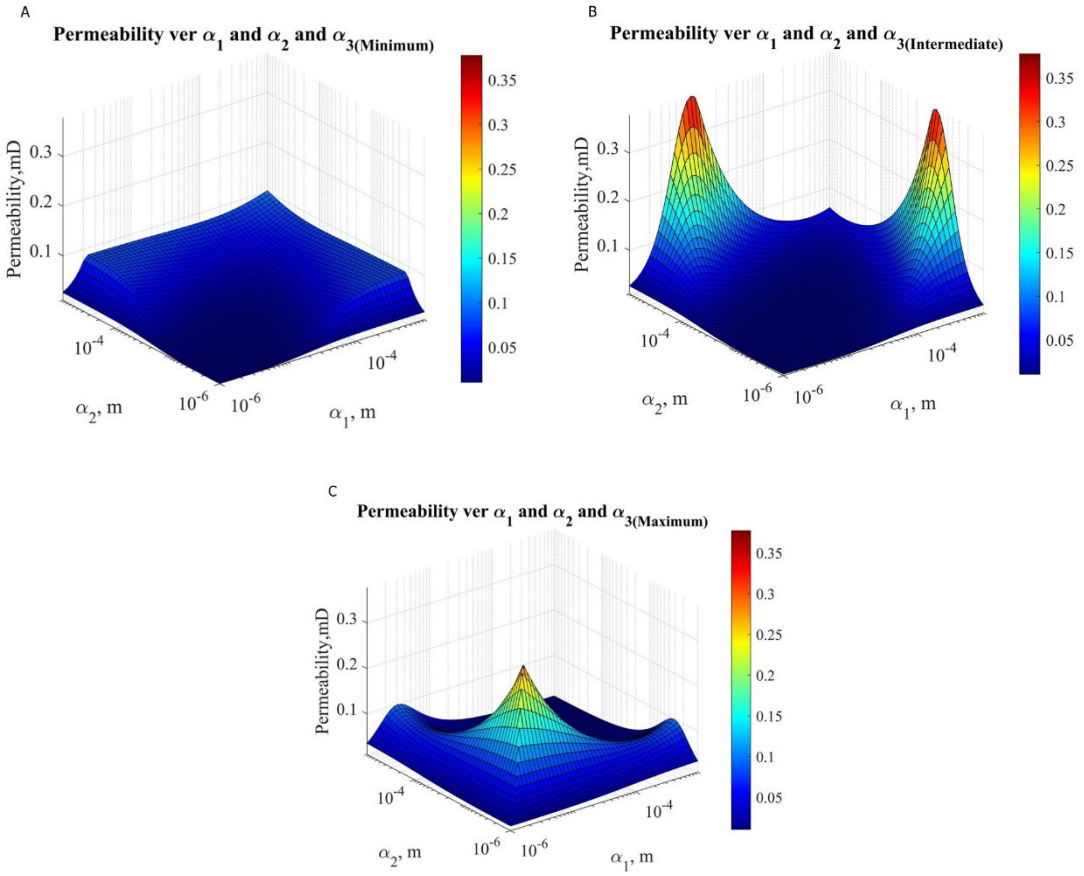

Figure 3. Permeability variations resulting from changes in aspect ratios are modeled using the T-matrix model. In order to maintain graphical consistency with other figures, we depict these changes by focusing on adjustments to the third semiaxis across minimal, intermediate, and maximal ranges. A: When the third semiaxis is at its minimum value, an increase in permeability is observed as aspect ratios are heightened in all directions. B: Within the intermediate range of the third semiaxis, the ellipsoidal form of fractures leads to the highest permeability values. C: As the third semiaxis reaches its maximal extent, permeability values stabilize within the midrange spectrum.

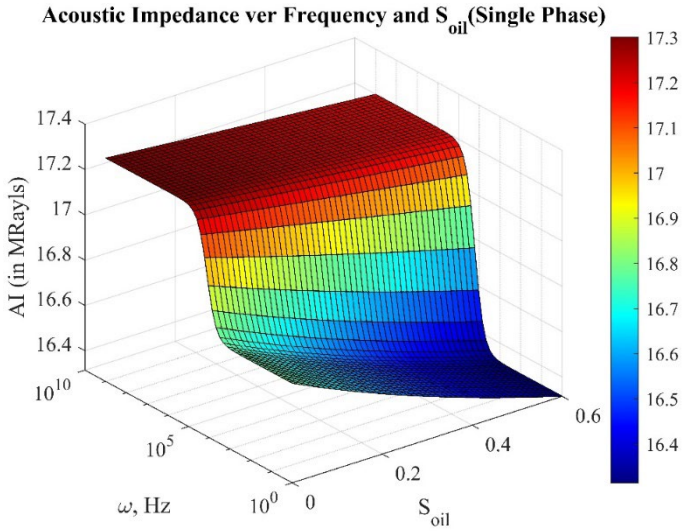

Figure 4. Acoustic Impedance versus the single-phase saturation in the range of seismic wave frequency to ultrasonic. This model is a tight carbonate fully saturated with oil and saline water.

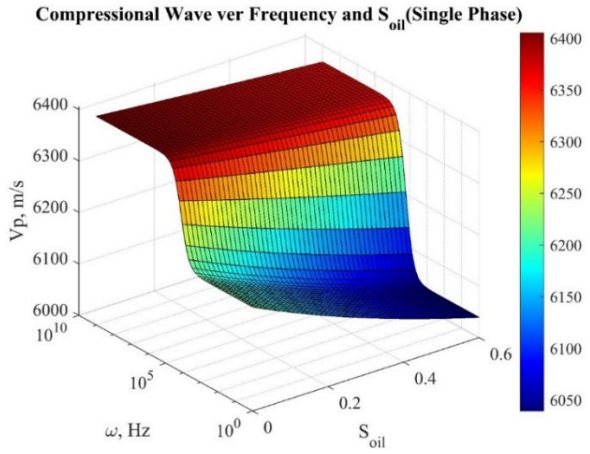

Figure 5. Velocity of compressional wave versus the single-phase saturation in the range of seismic wave frequency to ultrasonic. This model is a tight carbonate fully saturated with oil and saline water.

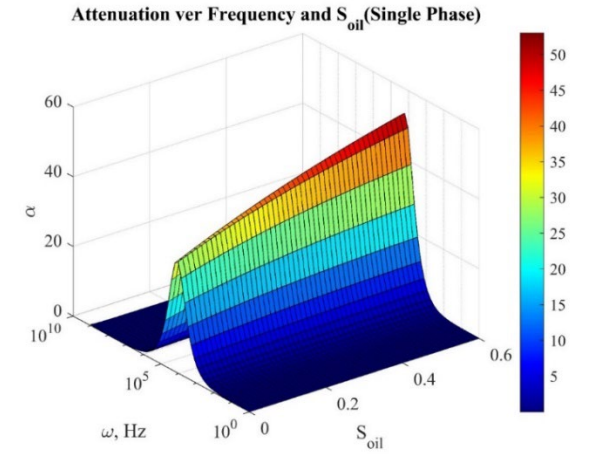

Figure 6. Attenuation of the compressional wave versus the single-phase saturation in the range of seismic wave frequency to ultrasonic. This model is a tight carbonate fully saturated with oil and saline water.

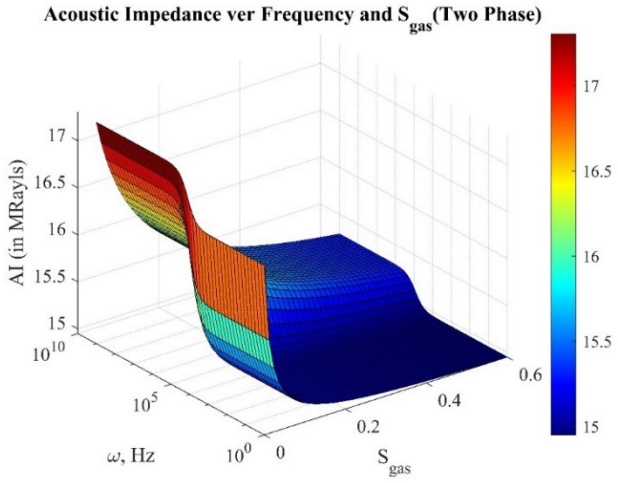

Figure 7. Acoustic Impedance versus the two-phase saturation in the range of seismic wave frequency to ultrasonic. This model is a tight carbonate fully saturated with oil and gas.

attenuation depends on fluid saturation and frequency. Therefore, this study emphasizes the importance of considering the frequency of seismic waves, with maximum attenuation occurring in the middle-frequency range (logging frequency). While these findings resonate with studies by with Liu et al., (2022) and Pang et al., (2019), our model provides a more distinct and prominent magnitude of attenuation.

Saturation in two-phase fluid:

Figure 7 illustrates changes in acoustic impedance due to frequency and fluid saturation in a two-phase fluid model. When an acoustic P-wave encounters the interface between different mediums, such as transitioning from solid to gas or fluid to gas, it undergoes reflection and refraction. The extent of reflection and refraction hinges on the acoustic impedance contrast between the two mediums. Gas often introduces a significant contrast, resulting in observable reflection and refraction. Since the fluid homogenization is aligned with Woods law, and the primary rigid carbonate medium is denser than the fluid in the cavities, alterations in fluid percentage do not affect acoustic impedance.

The relationship between velocity dispersion and frequency in two-phase flow generally follows a pattern similar to single-phase flow across various frequency ranges, with an exception observed in the 0-20% gas saturation range. In this specific range, depicted in Figure 8, an increase in gas content within the cavities leads to a substantial reduction in velocity magnitude, resulting in positive dispersion. This positive dispersion is attributed to the greater compressibility of gas compared to the fluid, creating a distinct pressure gradient during the passage of the primary acoustic wave

Figure 9 showcases variations in P-wave attenuation across a broad frequency range as two-phase saturation undergoes changes. The model effectively captures shifts in attenuation throughout gas saturation, particularly in the medium frequency range. Ba et al.'s findings (Ba et al., (2023)) align with the concept that variation in saturation impact attenuation. Their study indicates that higher oil saturation leads to increased attenuation, and water saturation causes more attenuation than gas saturation.

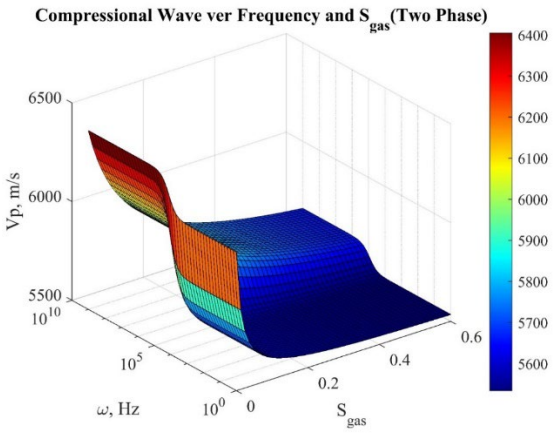

Figure 8. Velocity of compressional wave versus the two-phase saturation in the range of seismic wave frequency to ultrasonic. This model is a tight carbonate fully saturated with oil and gas.

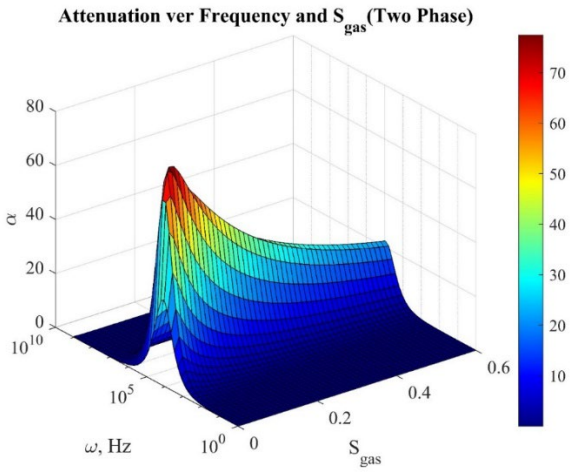

Figure 9. Attenuation of the compressional wave versus the two-phase saturation in the range of seismic wave frequency to ultrasonic. This model is a tight carbonate fully saturated with oil and gas.

Relaxation Time:

Figure 10 to Figure 12 provide visual representations of acoustic impedance, P-wave velocity, and attenuation in relation to relaxation time. Figure 11 illustrates the direct impact of relaxation time on velocity dispersion, showcasing strong positive dispersion in the ultrasonic frequency range within our model. As relaxation time increases, this dispersion in P-wave velocity shifts towards lower frequencies.

The trend observed in attenuation (Figure 12) aligns with that of velocity; the maximum attenuation occurs at the highest frequency and the shortest relaxation time, shifting towards lower frequencies with an increase in relaxation time. This trend is indicative of the fluid stiffness range at high frequencies, as depicted in Figure 11.

The model, particularly in the P-wave velocity and attenuation aspects, affirms that at high frequencies or short relaxation times, cracks exhibit behavior akin to a stiff embedding matrix, resulting in a decrease in attenuation and an increase in P-wave velocity. This observation is consistent with previous research findings like (Mavko and Jizba, 1991), Gurevich et al., (2010) and Alkhimenkov et al., (2020b). When a wave passes through saturated cracks, it induces pressure gradients, prompting fluid movement towards stiff pores to achieve pressure equilibration. This mechanism leads to robust energy dispersion, a process intricately tied to frequency dynamics.

In the low-frequency regime, the pressure gradient has sufficient time to equilibrate over half a cycle of the seismic wave, allowing for a straightforward modeling of the effective elastic moduli of the saturated medium using Gassman's model (Mavko and Jizba, 1991). Conversely, in the high-frequency regime, the fluid pressure gradient lacks adequate time for equilibration. Consequently, cracks become stiffer, exhibiting increased rigidity, with the fluid within the cracks assumed to be part of the frame materials (Mavko and Jizba, 1991).

The intermediate frequency regime introduces complexity in describing the crack response. The dependence of relaxation time on frequency signifies the saturated crack's evolving response to the incident P-wave. Consequently, it

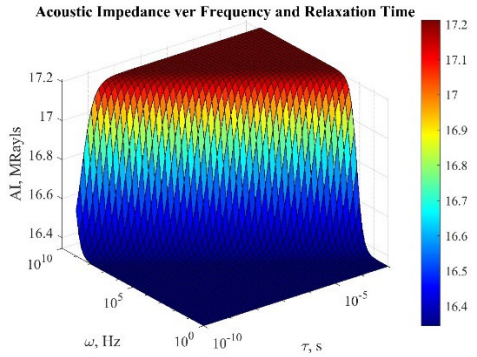

Figure 10. Acoustic Impedance versus relaxation time in the range of seismic wave frequency to ultrasonic.

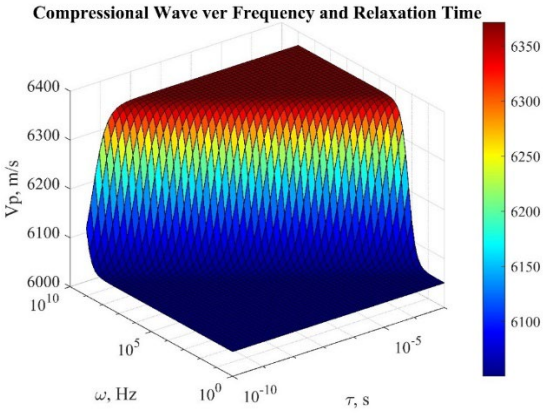

Figure 11. Velocity of compressional wave versus relaxation time in the range of seismic wave frequency to ultrasonic.

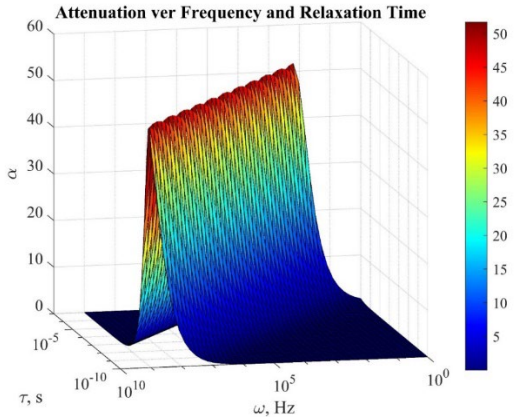

Figure 12. Attenuation of the compressional wave versus relaxation time in the range of seismic wave frequency to ultrasonic.

becomes stiffer as frequency increases, transitioning from relaxed to unrelaxed states, aligning seamlessly with our results for relaxation time.

Gurevich et al., (2010) argued that the effective stiffness of fractures in relaxed and unrelaxed states can be calculated using the frequency-dependent fluid bulk modulus $K_f^*(\omega)$. Alkhimenkov et al., (2020b) supported this notion under

the condition of $P_f = 0$ at the crack boundaries. Gurevich et al., (2010), however, applied boundary conditions solely to the walls of cracks, neglecting the stiffness of the pore space surrounding the cracks.

Ellipsoidal cracks:

Figure 13 to Figure 15 showcase variation in P-wave velocity and attenuation across different aspect ratios. In our model, the incident P-wave direction angle is set at zero, revealing that changes in the third semiaxis yield maximum attenuation. These figures are presented in three distinct ranges of the three semi-axes and three frequency ranges, spanning seismic to core sample frequencies.

The findings from these figures indicate that both P-wave velocity and attenuation are profoundly influenced by the morphology of elliposidal cracks. For instance, for spherical inclusions ($a_1 = a_2 = a_3$ or equivalently $\alpha_1 = \alpha_2 = 1$) (Figure 13-A, Figure 14-A, Figure 15-A), P-wave velocity reaches its zenith. However, as the cracks transition towards a penny shape, the velocity significantly decreases due to a reduction in the quality factor (Q), resulting in heightened attenuation. Conversely, when the third semiaxis falls within the middle range (Figure 13-B, Figure 14-B, Figure 15-B), variation in the other axes from oblate to prolate have minimal impact on the quality factor, velocity, and attenuation.

In the maximum range of the third semiaxis (Figure 13-C, Figure 14-C, Figure 15-C), if the minimum semi-axis of the penny shape fractures is oriented perpendicularly to the incident P-wave direction, a drastic drop in P-wave velocity occurs, accompanied by an increase in attenuation.

Figure 13 to Figure 15 present these graphical representations in three different frequency ranges, demonstrating the consistent performance of the proposed model across seismic to coring frequencies, with the most notable distinctions observed in the middle-frequency range.

Several models elucidate intrinsic attenuation through squirt flow, exploring its occurrence between connected elliposidal cracks((Murphy et al., 1991), (Dvorkin et al., 1994), , (Chapman et al., 2002), (Jakobsen and Chapman, 2009), (Müller et al., 2010), (Alkhimenkov et al., 2020b). Alkhimenkov and Quintal, (2021) have raised concerns about the simplicity of shapes used to represent squirt flows, asserting that they lack validation against computer-based solutions or exhibit limited accuracy. In essence, the reliability of the models they employ may be questionable or may not align well with real-medium scenarios. Building upon past studies, our model extends its scope to incorporate complex pore shapes, spanning from oblate to prolate with chaotic orientations. This inclusive model encompasses two categories of pores and cracks or fractures at the mesoscopic scale, where the crack aspect ratio varies from 10^{-6} m to 10^{-9} in chaotic orientation.

Model validation: The validation of theoretical rock physics models, particularly those predicting seismic attenuation, is critically dependent on high-quality experimental data. However, comprehensive laboratory measurements that concurrently provide detailed petrophysical properties, microstructural analysis, and attenuation spectra across a range of saturations are exceptionally scarce for carbonate rocks. Among the limited body of work, the study by (Adam et al., 2009) stands out

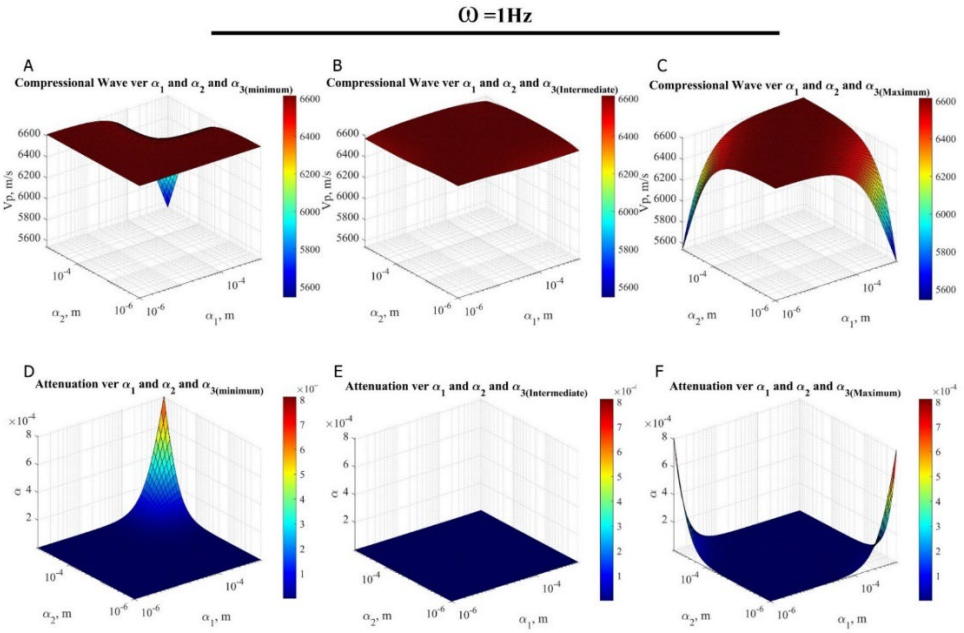

Figure 13. Velocity and attenuation of compressional wave response to aspect ratio variations of fractures in the seismic frequency range. A, D: In the minimum range of the 3rd semiaxis, with the same increase in the other semi-axes, the compressional wave velocity experiences a severe drop, accompanied by an increase in its attenuation. B, E: In the intermediate range of the 3rd semiaxis, changes in the other semi-axes do not result in significant variations in velocity and attenuation. C, F: In the maximum range of the 3rd semiaxis, when the incident P-wave is perpendicular to the minimum diameter of the pore, the velocity of the compressional wave sharply decreases, and its attenuation increases simultaneously.

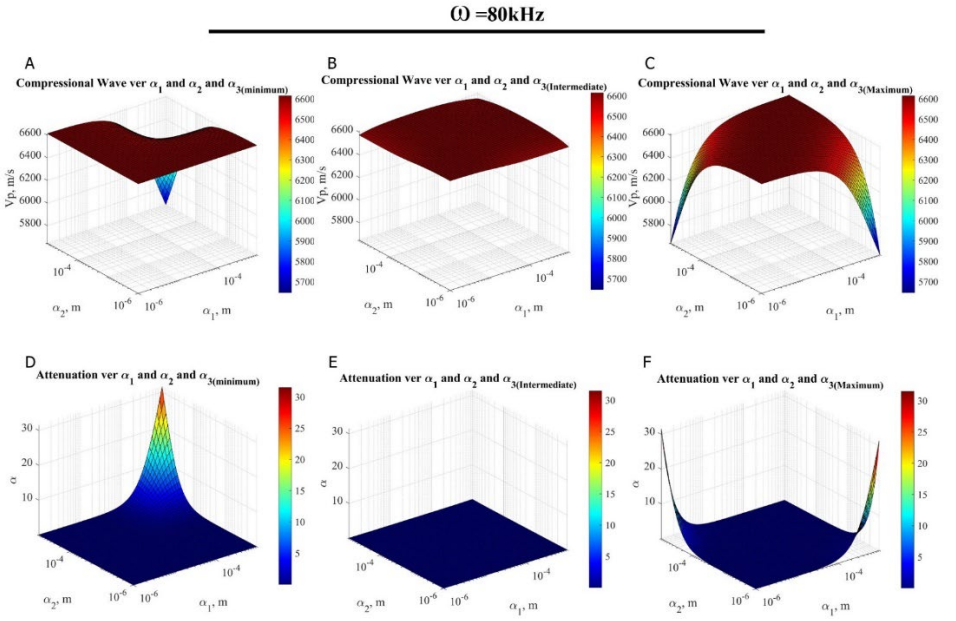

Figure 14. Velocity and attenuation of compressional wave response to aspect ratio variations of fractures in the logging frequency range. In all ranges of the 3rd semi-axes, we can observe similar results as in Figure 13, with the only difference being that the magnitude of the results in this frequency range is more prominent.

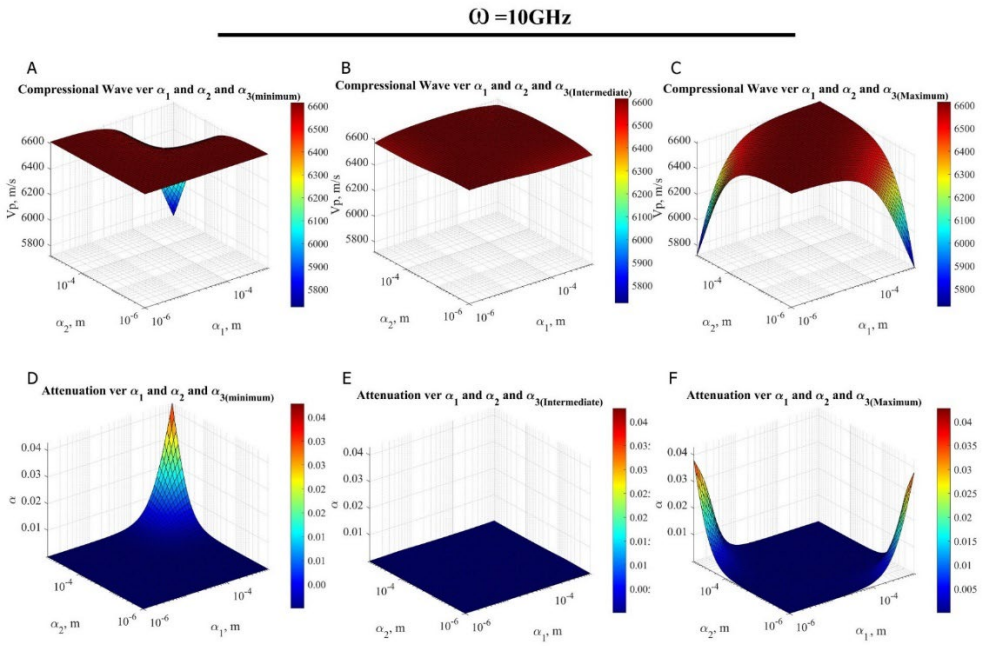

Figure 15. velocity and attenuation of compressional wave response to aspect ratio variations of fractures in the logging frequency range. In all ranges of the 3rd semi-axes, we can observe similar results as in Figure 13.

as a singularly complete and valuable dataset for model benchmarking. They provide a thorough petrophysical and microstructural characterization—including porosity, permeability, mineralogy, texture, and pore geometry from thin sections and SEM imagery—for five carbonate samples with varying heterogeneity. Crucially, they measured attenuation (1/Q) not only at ultrasonic frequencies but also across the seismic bandwidth (10–1000 Hz) under reservoir differential pressures, for both dry and fully saturated states (with brine and liquid butane). This rare combination of extensive sample characterization and broad-frequency, high-pressure attenuation measurements makes Adam et al. (2009) an ideal empirical standard against which to validate the predictions of our theoretical model. The validation process begans with inversion and solving for permeability to estimate crack aspect ratio. This estimated crack aspect ratio was then used as an input into equations 19–23 to compute a theoretical permeability value. Subsequently, both the estimated permeability and crack aspect ratio were incorporated into equations 12, 13, and 6–8. The final step involved solving the central T-matrix equation (Equation 1) to obtain the complex stiffness tensor. The seismic phase velocities were then derived from this tensor by solving Christoffel's equation. Finally, the quality factor (Q) was computed using Equation 24.

The results of the permeability inversion show excellent agreement with the experimentally measured values from {Adam et al., 2009} when a crack aspect ratio of 0.0001 is used (see Figure 16). Furthermore, Figure 17 demonstrates the successful application of the proposed algorithm to the experimental attenuation data. The model's predictions align closely with the measured quality factors for samples 100, 200, B, and C. As noted by Adam et al. (2009), sample 300 exhibits significant heterogeneity and contains larger cracks. This microstructural complexity justifies the

fair, though less perfect, validation result for this sample when using the T-matrix method. Effective medium theories, including the T-matrix approach, are predicated on the assumption that inclusion size is substantially smaller than the seismic wavelength. For larger inclusions, scattering becomes the dominant attenuation mechanism. Consequently, to more comprehensively model attenuation in porous fractured media, it is necessary to consider a multi-scale approach that integrates different physical mechanisms. A promising direction for future research would be to augment the current algorithm by incorporating multiple scattering effects, thereby investigating the relative contribution of different attenuation mechanisms across scales.(Adam et al., 2009).

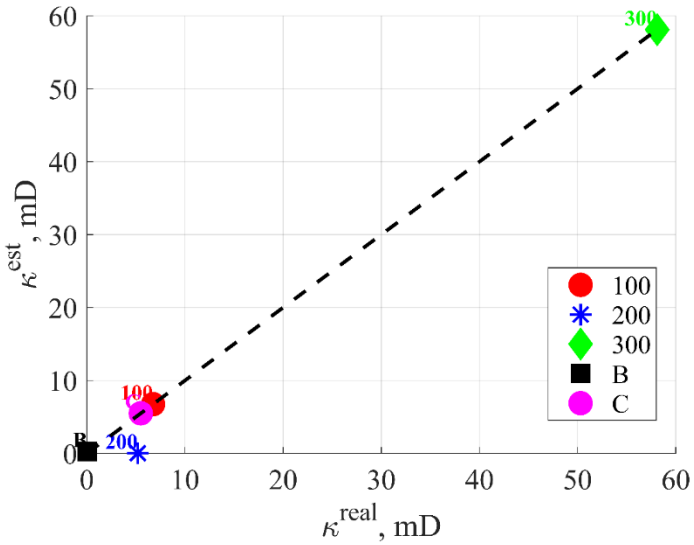

Figure 16. Real permeability versus predicted permeability of the samples provided in Adam's 2009 paper.

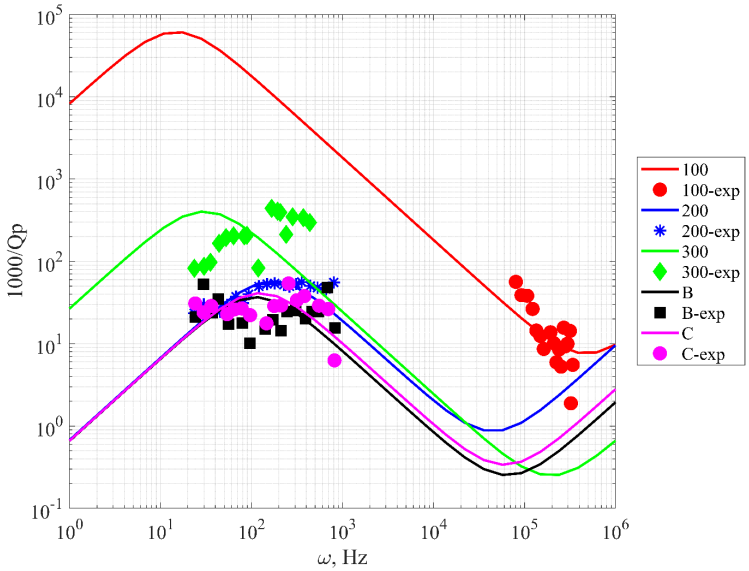

Figure 17. The predicted attenuation due to squirt flow (colored lines) versus experimental values (markers) obtained for sample "100" (red line and circle markers), sample "200" (blue line and star markers), sample "300" (green line and diamond markers), sample "B" (black line and squar markers), sample "C" (purple line and circle markers).

Wood's law and effect of patchy saturation: The use of Wood's law (equation 18) assumes a uniform, homogeneous mixing of fluids at the pore scale, which is a valid assumption for estimating the low-frequency elastic response of a fully saturated rock. However, it is important to acknowledge its limitation in neglecting 'patchy saturation,' a common scenario in carbonates where heterogeneous pore systems and wettability variations can lead to fluids being distributed in discrete, large patches. In such cases, the effective fluid modulus and subsequent seismic response would differ, often exhibiting higher velocities and less attenuation at seismic frequencies than predicted by a uniform mixing model white (Dutta and Seriff, 1979; White, 1975) .While the uniform saturation assumption is appropriate for this study's initial focus on integrating pore geometry and permeability into the squirt flow mechanism, the implications of patchy saturation represent a critical area for future extension of this model to enhance its applicability to real carbonate reservoirs with complex fluid distributions.

The t-matrix model limitations: The model presented in this study, grounded in the T-matrix approach and squirt-flow mechanics, provides a robust framework for predicting attenuation in media dominated by microcracks and small-scale pores. However, its applicability is inherently tied to the underlying assumption of a fully saturated, microcrack-dominated pore system. The presence of significant vuggy or macro-fracture networks would substantially alter the physical mechanisms governing wave propagation and attenuation. In vuggy carbonates, the attenuation mechanism would likely shift from local squirt flow to mesoscopic (Biot-type) fluid flow between stiff vugs and a compliant microporous matrix, characterized by a different relaxation frequency and reduced geometric anisotropy. Conversely, in rocks containing large, open fractures, scattering from wavelength-scale heterogeneities and channelized flow along fracture planes would become the dominant loss mechanisms, potentially leading to an underestimation of attenuation by the current model. Therefore, while this work offers significant insight into fluid-related dissipation in homogeneous microporous rocks, its predictions should be applied with caution to highly heterogeneous reservoirs. Future work should focus on developing a multi-porosity model that integrates the proposed squirt-flow formulation with mesoscopic loss and scattering theories to more comprehensively address the full spectrum of pore geometries encountered in complex carbonate reservoirs.

Conclusion

This study integrates theoretical modeling and sensitivity analyses to elucidate the complex relationships among pore geometry, fluid saturation, and seismic wave properties in tight carbonate rocks. By leveraging the T-matrix formulation, we demonstrate that hydraulic permeability is maximized in prolate-shaped ellipsoidal cracks, with variations in pore aspect ratios and fluid content exerting significant control over seismic velocity, attenuation, and dispersion. Single-phase fluid models reveal that higher oil saturation amplifies attenuation, particularly within logging frequencies, while gas saturation in two-phase systems induces pronounced

velocity reduction due to compressibility contrasts. The role of relaxation time emerges as pivotal in governing frequency-dependent behavior, with high-frequency regimes stiffening cracks and suppressing attenuation, consistent with squirt flow dynamics and Gassman's framework. Our analysis of ellipsoidal crack morphologies further highlights how velocity minima and attenuation maxima arise when cracks align perpendicularly to wave propagation, particularly in penny-shaped geometries. These findings align with prior studies but refine predictions by incorporating chaotic pore orientations and complex saturation scenarios, addressing limitations of oversimplified pore models. The results underscore the necessity of integrating microstructure, fluid heterogeneity, and frequency effects into seismic interpretations. This work advances the predictive modeling of hydraulic and elastic properties in carbonates, offering a bridge between theoretical rock physics and practical subsurface applications.

The model was validated against experimental data from Adam et al. (2009), demonstrating close agreement between predicted and measured permeability and attenuation values for homogeneous samples. However, predictions for a heterogeneous sample deviated, likely due to the presence of larger-scale features where scattering dominates over squirt-flow mechanisms.

A key contribution of this work is the direct microstructurally-based coupling between permeability and dynamic squirt-flow response, addressing a gap in existing models for fractured carbonates. The findings highlight the influence of pore geometry and frequency-dependent fluid mobility on seismic attributes.

To address the limitations and extensions identified in this study, future work will focus on developing a more comprehensive multi-scale attenuation model. This effort will proceed in three key directions:

- Incorporating Patchy Saturation: The current model, which uses Wood's Law for fluid homogenization, assumes uniform fluid mixing at the pore scale. To model patchy saturation, where fluids are heterogeneously distributed in mesoscopic patches, we will integrate the White or Dutta-Seriff model into our framework. This involves calculating a frequency-dependent effective fluid modulus ($K_f^*(\omega)$) that accounts for the wave-induced fluid flow between patches of different fluids. This modulus would then replace the homogenous K_f in the current T-matrix formulation for the inclusions.
- Multi-Scale Pore Space Inclusion: The model will be extended to handle a more realistic pore geometry consisting of multiple inclusion types (e.g., spheres for vugs, penny-shaped cracks for microcracks, and needles for macropores). This will be achieved by defining separate T-matrices for each pore type within the same effective medium scheme, allowing us to quantify the individual and combined contributions of different pore scales to the overall seismic response.
- Impact of Multiple Scattering: For media containing large-scale heterogeneities (e.g., macro-fractures or vugs comparable to the wavelength), a scattering operator will be developed and coupled with the current intrinsic attenuation model. This will involve separating the total attenuation (Q_{total}^{-1}) into intrinsic ($Q_{intrinsic}^{-1}$) and scattering ($Q_{scattering}^{-1}$) components, where the intrinsic part is derived from the current model and the scattering part is estimated

using methods like the Foldy approximation for discrete scatterers.

By pursuing these specific avenues, we aim to create a unified model capable of predicting attenuation across a broader range of reservoir conditions and complexities.

References

Adam, L., M. Batzle, K. T. Lewallen, and K. van Wijk, 2009, Seismic wave attenuation in carbonates: Journal of Geophysical Research: Solid Earth, **114**, no. B6. http://dx.doi.org/https://doi.org/10.1029/2008JB005890.

Alkhimenkov, Y., and B. Quintal, 2021, An accurate analytical model for squirt flow in anisotropic porous rocks - Part 1: Classical geometry: GEOPHYSICS, **87**, 1-81. http://dx.doi.org/10.1190/geo2021-0229.1.

Alkhimenkov, Y., and B. Quintal, 2024, A simple and accurate model for attenuation and dispersion caused by squirt flow in isotropic porous rocks: GEOPHYSICS, **89**, no. 1, MR1-MR10.

Alkhimenkov, Y., E. Caspari, S. Lissa, and B. Quintal, 2020a, Azimuth-, angle-and frequency-dependent seismic velocities of cracked rocks due to squirt flow: Solid Earth, **11**, no. 3, 855-871.

Alkhimenkov, Y., E. Caspari, B. Gurevich, N. D. Barbosa, S. Glubokovskikh, J. Hunziker, and B. Quintal, 2020b, Frequency-dependent attenuation and dispersion caused by squirt flow: Three-dimensional numerical study: GEOPHYSICS, **85**, no. 3, MR129-MR145. http://dx.doi.org/10.1190/geo2019-0519.1.

Ba, J., X. Pan, J. M. Carcione, and R. Ma. 2023, Effects of pressure and fluid properties on P-wave velocity and attenuation of tight sandstones. Paper read at Frontiers in Earth Science.

Ba, J., Y. Wei, J. M. Carcione, L. Adam, and G. Tang, 2024, Stress and frequency dependence of wave velocities in saturated rocks based on acoustoelasticity with squirt-flow dissipation: Geophysical Journal International, **236**, no. 3, 1753-1763.

Barthélémy, J. F., 2009, Effective Permeability of Media with a Dense Network of Long and Micro Fractures: Transport in Porous Media, **76**, no. 1, 153-178. http://dx.doi.org/10.1007/s11242-008-9241-9.

Bayuk, I., and E. Chesnokov, 1998, Correlation between elastic and transport properties of porous cracked anisotropic media: Physics and Chemistry of the Earth, **23**, no. 3, 361-366.

Biot, M. A., 1956, Theory of Propagation of Elastic Waves in a Fluid-Saturated Porous Solid. II. Higher Frequency Range: The Journal of the Acoustical Society of America, **28**, no. 2, 179-191. http://dx.doi.org/10.1121/1.1908241.

Buckingham, M. J., 2000, Wave propagation, stress relaxation, and grain-to-grain shearing in saturated, unconsolidated marine sediments: The Journal of the Acoustical Society of America, **108**, no. 6, 2796-2815. http://dx.doi.org/10.1121/1.1322018.

Carcione, J. M., F. Poletto, and B. Farina, 2018a, The Burgers/squirt-flow seismic model of the crust and mantle: Physics of the Earth and Planetary Interiors, **274**, 14-22.

Carcione, J. M., Z.-W. Wang, W. Ling, E.

Salusti, J. Ba, and L.-Y. Fu, 2018b, Simulation of wave propagation in linear thermoelastic media: GEOPHYSICS, **84**, no. 1, T1-T11. http://dx.doi.org/10.1190/geo2018-0448.1.

Chapman, M., S. V. Zatsepin, and S. Crampin, 2002, Derivation of a microstructural poroelastic model: Geophysical Journal International, **151**, no. 2, 427-451. http://dx.doi.org/10.1046/j.1365-246X.2002.01769.x.

Chen, Y., Z. Zong, and H. Zhu, 2022, Biot-spherical squirt (BISSQ) model for wave attenuation and dispersion: Geophysical Journal International, **231**, no. 2, 1138-1149.

Coulman, T., W. Deng, and I. Morozov, 2013, Models of seismic attenuation measurements in the laboratory: Canadian Journal of Exploration Geophysics, **38**, 51-67.

Diallo, M. S., and E. Appel, 2000, Acoustic wave propagation in saturated porous media: reformulation of the Biot/Squirt flow theory: Journal of Applied Geophysics, **44**, no. 4, 313-325. http://dx.doi.org/https://doi.org/10.1016/S0926-9851(00)00009-4.

Dutta, N. C., and A. J. Seriff, 1979, On White's model of attenuation in rocks with partial gas saturation: GEOPHYSICS, **44**, no. 11, 1806-1812. http://dx.doi.org/10.1190/1.1440940.

Dvorkin, J., R. Nolen-Hoeksema, and A. Nur, 1994, The squirt-flow mechanism: Macroscopic description: GEOPHYSICS, **59**, no. 3, 428-438. http://dx.doi.org/10.1190/1.1443605.

Farla, R. J. M., I. Jackson, J. D. Fitz Gerald, U. H. Faul, and M. E. Zimmerman, 2012, Dislocation Damping and Anisotropic Seismic Wave Attenuation in Earth's Upper Mantle: science, **336**, no. 6079, 332-335. http://dx.doi.org/10.1126/science.1218318.

Fokker, P. A., 2001, General Anisotropic Effective Medium Theory for the Effective Permeability of Heterogeneous Reservoirs: Transport in Porous Media, **44**, no. 2, 205-218. http://dx.doi.org/10.1023/A:1010770623874.

Goetze, C., 1977, Bounds on the subsolidus attenuation for four rock types at simultaneous high temperature and pressure: Tectonophysics, **42**, no. 1, T1-T5.

Gueguen, Y., J. Woirgard, and M. Darot, 1981, Attenuation mechanisms and anelasticity in the upper mantle: Anelasticity in the Earth, **4**, 86-94.

Gurevich, B., D. Makarynska, O. B. de Paula, and M. Pervukhina, 2010, A simple model for squirt-flow dispersion and attenuation in fluid-saturated granular rocks: GEOPHYSICS, **75**, no. 6, N109-N120. http://dx.doi.org/10.1190/1.3509782.

Hudson, J. A., E. Liu, and S. Crampin, 1996, The mechanical properties of materials with interconnected cracks and pores: Geophysical Journal International, **124**, no. 1, 105-112. http://dx.doi.org/https://doi.org/10.1111/j.1365-246X.1996.tb06355.x.

Jackson, D. D., 1971, Attenuation of Seismic Waves by Grain Boundary Relaxation: Proceedings of the National Academy of Sciences, **68**, no. 7, 1577-1579. http://dx.doi.org/10.1073/pnas.68.7.1577.

Jackson, I., and M. Paterson, 1993, A high-pressure, high-temperature

apparatus for studies of seismic wave dispersion and attenuation: Pure and applied geophysics, **141**, 445-466.

Jackson, I., M. Paterson, and J. Fitz Gerald, 1992, Seismic wave dispersion and attenuation in Åheim dunite: an experimental study: Geophysical Journal International, **108**, no. 2, 517-534.

Jakobsen, M., 2006, The effective permeability of fractured reservoirs and composite porous media: Seg Technical Program Expanded Abstracts, **25**. http://dx.doi.org/10.1190/1.2369861.

Jakobsen, M., 2007, Effective hydraulic properties of fractured reservoirs and composite porous media: Journal of Seismic Exploration, **16**, 199-224.

Jakobsen, M., and J. A. Hudson, 2003, Visco-Elastic Waves in Rock-Like Composites: Studia Geophysica et Geodaetica, **47**, no. 4, 793-826. http://dx.doi.org/10.1023/A:1026394819263.

Jakobsen, M., and M. Chapman, 2009, Unified theory of global flow and squirt flow in cracked porous media: GEOPHYSICS, **74**, no. 2, WA65-WA76. http://dx.doi.org/10.1190/1.3078404.

Jakobsen, M., T. A. Johansen, and C. McCann, 2003, The acoustic signature of fluid flow in complex porous media: Journal of Applied Geophysics, **54**, no. 3, 219-246. http://dx.doi.org/https://doi.org/10.1016/j.jappgeo.2002.11.004.

Kjartansson, E., 1979, Constant Q-wave propagation and attenuation: Journal of Geophysical Research: Solid Earth, **84**, no. B9, 4737-4748. http://dx.doi.org/https://doi.org/10.1029/JB084iB09p04737.

Lan, T., Z. Zong, and Y. Feng, 2023, An improved seismic fluid identification method incorporating squirt flow and frequency-dependent fluid-solid inversion: Interpretation, **11**, no. 1, T117-T130.

Li, L., 2010, Bulk attenuation in the earth's mantle due to phase transitions: Physics of the Earth and Planetary Interiors, **183**, no. 3, 473-477. http://dx.doi.org/https://doi.org/10.1016/j.pepi.2010.09.012.

Liu, J., and W.-A. Yong, 2016, Stability analysis of the Biot/squirt models for wave propagation in saturated porous media: Geophysical Journal International, **204**, no. 1, 535-543. http://dx.doi.org/10.1093/gji/ggv463.

Liu, P., H. Huang, L. Hu, S. Mao, Z. Tian, and Y. Shen, 2022, Hydrate Attenuation Characteristics Based on the Patchy-Saturation Model: Frontiers in Earth Science, **10**. http://dx.doi.org/10.3389/feart.2022.831405.

Mavko, G., and A. Nur, 1975, Melt squirt in the asthenosphere: Journal of Geophysical Research (1896-1977), **80**, no. 11, 1444-1448. http://dx.doi.org/https://doi.org/10.1029/JB080i011p01444.

Mavko, G., T. Mukerji, and J. Dvorkin, 2020, The Rock Physics Handbook: Cambridge University Press.

Mukerji, T., and G. Mavko, 1994, Pore fluid effects on seismic velocity in anisotropic rocks: GEOPHYSICS, **59**, no. 2, 233-244. http://dx.doi.org/10.1190/1.1443585.

Müller, T. M., B. Gurevich, and M. Lebedev, 2010, Seismic wave attenuation and dispersion resulting from wave-induced flow in porous rocks — A review: GEOPHYSICS, **75**, no. 5, 75A147-175A164. http://dx.doi.org/10.1190/1.3463417.

Murphy, W. F., L. M. Schwartz, and B.

Hornby, 1991, Interpretation Physics Of Vp And Vs In Sedimentary Rocks.

Quintal, B., H. Steeb, M. Frehner, and S. M. Schmalholz, 2011, Quasi-static finite element modeling of seismic attenuation and dispersion due to wave-induced fluid flow in poroelastic media: Journal of Geophysical Research: Solid Earth, **116**, no. B1.

Ricard, Y., J. Matas, and F. Chambat, 2009, Seismic attenuation in a phase change coexistence loop: Physics of the Earth and Planetary Interiors, **176**, no. 1, 124-131. http://dx.doi.org/https://doi.org/10.1016/j.pepi.2009.04.007.

Sævik, P. N., I. Berre, M. Jakobsen, and M. Lien, 2012, Electrical conductivity of fractured media: A computational study of the self-consistent method, SEG Technical Program Expanded Abstracts 2012: Society of Exploration Geophysicists SEG Technical Program Expanded Abstracts, 1-5.

Sævik, P. N., I. Berre, M. Jakobsen, and M. Lien, 2013, A 3D Computational Study of Effective Medium Methods Applied to Fractured Media: Transport in Porous Media, **100**, no. 1, 115-142. http://dx.doi.org/10.1007/s11242-013-0208-0.

Sævik, P. N., M. Jakobsen, M. Lien, and I. Berre, 2014, Anisotropic effective conductivity in fractured rocks by explicit effective medium methods: Geophysical Prospecting, **62**, no. 6, 1297-1314. http://dx.doi.org/https://doi.org/10.1111/1365-2478.12173.

Sato, H., 1984, Attenuation and envelope formation of three-component seismograms of small local earthquakes in randomly inhomogeneous lithosphere: Journal of Geophysical Research: Solid Earth, **89**, no. B2, 1221-1241.

Savage, J. C., 1966, Thermoelastic attenuation of elastic waves by cracks: Journal of Geophysical Research (1896-1977), **71**, no. 16, 3929-3938. http://dx.doi.org/https://doi.org/10.1029/JZ071i016p03929.

Solazzi, S. G., L. Bodet, K. Holliger, and D. Jougnot, 2021, Surface-wave dispersion in partially saturated soils: The role of capillary forces: Journal of Geophysical Research: Solid Earth, **126**, no. 12, e2021JB022074.

Subramaniyan, S., B. Quintal, C. Madonna, and E. H. Saenger, 2015, Laboratory-based seismic attenuation in Fontainebleau sandstone: Evidence of squirt flow: Journal of Geophysical Research: Solid Earth, **120**, no. 11, 7526-7535.

Sun, Y., J. M. Carcione, and B. Gurevich, 2020, Squirt-flow seismic dispersion models: a comparison: Geophysical Journal International, **222**, no. 3, 2068-2082.

Torquato, S., 2002, Effective-Medium Approximations, *in* S. Torquato, ed., Random Heterogeneous Materials: Microstructure and Macroscopic Properties: Springer New York, 459-484.

White, J. E., 1975, COMPUTED SEISMIC SPEEDS AND ATTENUATION IN ROCKS WITH PARTIAL GAS SATURATION: GEOPHYSICS, **40**, no. 2, 224-232. http://dx.doi.org/10.1190/1.1440520.

Wood, A. B., 1957, A Textbook of Sound: Being an Account of the Physics of Vibrations with Special Reference to Recent Theoretical and Technical Developments: G. Bell.

Yang, Y., D. W. Forsyth, and D. S.

Weeraratne, 2007, Seismic attenuation near the East Pacific Rise and the origin of the low-velocity zone: Earth and Planetary Science Letters, **258**, no. 1-2, 260-268.